Analytic Corrections to CFD Heating Predictions Accounting for Changes in Surface Catalysis, Part II

Peter A. Gnoffo *
NASA Langley Research Center
Hampton, Virginia 23681-0001
and
George R. Inger†
Iowa State University
Ames, Iowa 50011-3231

Abstract

A new approach for combining the insight afforded by integral boundary-layer analysis with comprehensive (but time intensive) computational fluid dynamic (CFD) flowfield solutions of the thin-layer Navier-Stokes equations is described. The approach extracts CFD derived quantities at the wall and at the boundary layer edge for inclusion in a post-processing boundary-layer analysis. It allows a designer at a workstation to address two questions, given a *single* CFD solution. (1) How much does the heating change for a thermal protection system (TPS) with different catalytic properties than was used in the original CFD solution? (2) How does the heating change at the interface of two different TPS materials with an abrupt change in catalytic efficiency? The answer to the second question is particularly important, because abrupt changes from low to high catalytic efficiency can lead to localized increase in heating which exceeds the usually conservative estimate provided by a fully catalytic wall assumption. Capabilities of this approach for application to Reusable Launch Vehicle (RLV) design are demonstrated. If the definition of surface catalysis is uncertain early in the design process, results show that fully catalytic wall boundary conditions provide the best baseline for CFD design points.

Nomenclature

C	relaxation coefficient in Method 2
C_D	equilibrium constant, $p_e e^{\theta_D} \left[\frac{\alpha_e^2}{1.-\alpha_e^2}\right]_{EQ}$
$\hat{C}_p$	specific heat of molecules, J/kmole-K
h	enthalpy per unit mass of mixture, J/kg
h_D	heat of formation per unit mass of species, J/kg
$I_{(1-3,D)}$	reaction integrals
k_r	recombination rate coefficient, m^6/kmole^2-s
Le	Lewis number
p	pressure, N/m^2
Pr	Prandtl number
q	surface heating, W/m^2
Q	heat transfer function
r	ratio of velocity gradients
R	radius of curvature, m
R_s	gas constant for species s, J/kmole-K
R_u	univ. gas constant, 8314.3 J/kmole-K
Sc	Schmidt number
T	temperature, K
T_D	characteristic temperature of dissociation, K
u, w	streamwise and crossflow velocities, m/s
V	total velocity, m/s
x, z	streamwise and crossflow distances, m
Z	bridging function
α	mass fraction of atoms
γ	catalytic efficiency of surface
Γ^*	composite Dahmkohler number
$\Gamma_c, \tilde{\Gamma}_c$	Dahmkohler numbers for surface catalysis
Γ_D	Dahmkohler number for dissociation dominated flow
Γ_G	Dahmkohler number for recombination dominated flow
ρ	density, kg/m^3
μ	viscosity, N-s/m^2
θ	temperature ratio T/T_e
θ_D	temperature ratio T_D/T_e
ξ, η	Levy-Lees transformation coordinates
χ	parameter $u_e(d\xi/dx)(1+r)/\xi$, 1/s

*Aerospace Engineer, Aerothermodynamics Branch, Aero- and Gas-Dynamics Division, Associate Fellow AIAA.

†Professor, Dept. of Aerospace Engr. & Engr. Mechanics, Associate Felow AIAA

Superscripts

$+$	value immediately following jump
$-$	value immediately preceding jump

Subscripts

∞	free stream
0	computed using $\gamma = 0$
1	computed using $\gamma = 1$
e	boundary-layer edge
EQ	equilibrium
F	frozen
i, j	CFD mesh point location
J	location of jump in surface catalysis
N	nitrogen atom
O	oxygen atom
w	wall
γ	computed using $\gamma = \gamma(T)$
$\gamma \rightarrow 1$	computed across discontinuity in γ from $\gamma = \gamma(T)$ to $\gamma = 1$

Algorithm Designation

Method 1	Continuous change of catalysis, restricted to nose region
Method 1G	Continuous change of catalysis, generalized validity
Method 2	Discontinuous change of catalysis, restricted to nose region
Method 2G	Discontinuous change of catalysis, generalized validity

Introduction

The grand challenge of Computational Fluid Dynamics (CFD) is to produce accurate solutions on real configurations in a matter of minutes. However, the reality of CFD simulation today is that computational expense and the complexity of surface definition and grid generation restricts the number of cases which can be produced. Given this limitation, a challenge often overlooked by the CFD community concerns the timely transmission and efficient utilization of the CFD solution(s) by all members of a vehicle design team. Recent experiences with the Phase I design process for X33 have revealed opportunities for development of software to better exploit a limited CFD solution matrix. Extraction of only a few parameters at the surface and at the boundary-layer edge of a CFD solution can enable analytic extension of heat transfer solutions beyond the baseline matrix.

Integral boundary-layer solution techniques applicable to the problem of determining aerodynamic heating rates of hypersonic vehicles in the vicinity of stagnation points, windward centerlines, and swept-wing leading edges are discussed in the literature.[1–4] The analyses include effects of finite-rate gas chemistry across the boundary layer and finite-rate catalysis of atom recombination at the surface. A new approach for combining the insight afforded by integral boundary-layer analysis with comprehensive (but time intensive) CFD flowfield solutions of the thin-layer Navier-Stokes equations is described. The approach extracts CFD derived quantities at the wall and at the boundary layer edge for inclusion in a post-processing boundary-layer analysis. The post-processed data base allows a designer at a workstation to address two questions, given a *single* CFD solution. (1) How much does the heating change for a thermal protection system with different catalytic properties than was used in the original CFD solution? (2) How does the heating change at the interface of two different TPS materials with an abrupt change in catalytic efficiency? The answer to the second question is particularly important, because abrupt changes from low to high catalytic efficiency can lead to localized increase in heating which exceeds the usually conservative estimate provided by a fully catalytic wall assumption. For a given trajectory point, the approach uses a single CFD solution obtained with a known variation of catalytic efficiency over the vehicle surface. Changes to CFD baseline heating levels are calculated as a function of changes in catalytic efficiency derived from integral boundary-layer solution techniques that utilize CFD generated edge and wall conditions.

The present paper reviews and extends work presented in an earlier report.[5] A reformulation of Method 1G[5] (see Nomenclature) is developed that better models the different roles of oxygen and nitrogen chemistry across the boundary layer and at the wall. The test cases focus on flow over a sphere at several trajectory points characteristic of reentry of a representative winged Single Stage to Orbit (SSTO) vehicle. CFD calculations are made for three wall catalysis models at each of these points. The models include noncatalytic, finite catalytic (Shuttle tile), and fully catalytic wall boundary conditions. The post processed integral boundary-layer corrections using each of three baseline CFD heating results are compared to actual CFD calculations for the corresponding off-baseline case. The results of tests using the same reformulation of Method 1G on vehicles of realistic geometric complexity appropriate for a Reusable Launch Vehicle (RLV) are presented. Relative differences in predicted heating levels between single CFD runs with post-processed correc-

tions and multiple CFD runs using different wall catalysis models are discussed. Finally, more comprehensive grid convergence studies have been provided for the case of abrupt change in surface catalysis using Method 2G.

The goal of this research is to create a stand-alone post-processing tool which can be used in preliminary design of thermal protection systems (TPS) for hypersonic vehicles. The tool would make extensive use of a small number of CFD solutions computed using a relatively simple surface catalysis model. Design iterations are conducted without need of additional CFD runs until convergence on a single concept is achieved, at which point CFD should be used to provide a final check and/or recalibration point.

Baseline CFD Solution Algorithm

The computational fluid dynamic (CFD) baseline solutions for real gas, viscous analysis are provided by the Langley Aerothermodynamic Upwind Relaxation Algorithm (LAURA).[6–8] Comparisons to experimental data for hypersonic flows in air are documented in the literature.[9–13] The code employs upwind-biased, point-implicit relaxation. Inviscid fluxes are approximated with Roe's averaging,[14] eigenvalue limiting (similar to Harten[15]), and Yee's symmetric total variation diminishing scheme.[16] Viscous fluxes are approximated with central differences. A model for surface catalytic efficiency[17] $\gamma(T)$ used in the present work is defined by

$$\begin{aligned} \gamma_O &= 40.e^{-11440./T_w} && 1435 < T_w < 1580 \\ \gamma_O &= 39.9\ 10^{-9} e^{21410./T_w} && 1580 < T_w < 1845 \\ \gamma_N &= 0.061 e^{-2480./T_w} && 1410 < T_w < 1640 \\ \gamma_N &= 0.00061 e^{5090./T_w} && 1640 < T_w < 1905 \end{aligned} \tag{1}$$

The catalytic recombination rate $K_{w,s}$ for species s is then defined by

$$K_{w,s} = \gamma_s(T_w)\sqrt{R_s T_w/2\pi} \tag{2}$$

Integral Boundary-Layer Method

Highlights

Integral boundary-layer theory for evaluating nonequilibrium effects on surface heating has been described previously.[2–4] Key features of the analysis are reviewed here. First, the model accounts for both finite catalysis of the surface and finite reactivity of the boundary layer. The finite catalysis of the surface enters the analysis through the Dahmkohler number, Γ_c, the ratio of atom recombination time at the surface and a characteristic local diffusion time.

$$\Gamma_c = \left[\frac{\rho_w}{\mu_w \chi}\right]^{1/2} Sc K_w \tag{3}$$

The finite reactivity of the boundary layer enters the analysis through the Dahmkohler number, Γ_G, and Γ_D the ratio of characteristic local flow time to gas phase reaction time. In the case of recombination dominated boundary layers (near stagnation points)

$$\Gamma_G = \frac{2 k_r T_e^{-2} p_e^2}{R_u^2 \chi} \tag{4}$$

In the case of dissociation dominated boundary layers (near windside centerline where viscous shear raises temperatures in the boundary layer)

$$\Gamma_D = \frac{C_D}{p_e}\Gamma_G \tag{5}$$

Second, analytic solutions to the governing boundary-layer equations can be made with simplifying approximations in the vicinity of the vehicle stagnation point (nose region), swept leading edge region, and windward centerline region. The parameter χ,

$$\chi = u_e (d\xi/dx)(1+r)/(2\xi) \tag{6}$$

is a function of the Levy-Lees transformed coordinate ξ and takes on relatively simple, limiting values in these regions. The Levy-Lees transformed coordinate is defined by

$$\xi = \int_0^x \rho_w \mu_w u_e dx. \tag{7}$$

Three-dimensional effects are included with the parameter $1+r$, where r is the ratio of velocity gradients at the edge of the boundary layer.

$$r = (dw_e/dz)/(du_e/dx) \tag{8}$$

The post-processing algorithm used to correct for changes in surface heating associated with global change of the surface catalysis model over a hypersonic vehicle is denoted Method 1. The initial formulation of Method 1[5] was restricted to the nose region because of the need to utilize a simple, analytic relation for χ. Subsequent modifications denoted by Method 1G are presented here which are more generally applicable to the complete vehicle surface. The post-processing algorithm used to correct for changes in surface heating associated with local, abrupt changes in surface catalysis in the nose region is denoted Method 2. It too has been modified to remove the requirement for an analytic definition of χ.

Global Change of Catalysis - Method 1G

Surface heating beneath a recombination dominated boundary layer can be expressed[2] as an appropriate interpolation of an equilibrium boundary-layer heating rate $Q_{w,EQ}$ and a frozen boundary-layer heating rate $Q_{w,F}$ by

$$Q_w = Q_{w,EQ} + Z(\Gamma^*)(Q_{w,F} - Q_{w,EQ}) \quad (9)$$

In Eq. 9 the variable Q is a dimensionless heating rate, related to the dimensional heating rate q_w by

$$Q_w = q_w \frac{-Pr/\hat{C}_p T_e}{\sqrt{\rho_w \mu_w \chi}} \quad (10)$$

The equilibrium boundary-layer heating rate $Q_{w,EQ}$ reference value at each mesh point (i,j) on a discretized vehicle surface is defined[2] by

$$Q_{w,EQ,i,j} = 0.47 Pr_{w,i,j}^{1/3} \left(1 - \theta_w + \sqrt{Pr_w}\frac{u_e^2}{2\hat{C}_p T_e} + Le_w^{0.52}\frac{\alpha_e h_D}{\hat{C}_p T_e}\right)_{i,j} \quad (11)$$

The reference value for frozen boundary-layer heating rate $Q_{w,F}$ at each mesh point (i,j) is defined[18] by

$$Q_{w,F,i,j} = 0.47 Pr_{w,i,j}^{1/3} \left(1 - \theta_w + \sqrt{Pr_w}\frac{u_e^2}{2\hat{C}_p T_e} + Le_w^{0.67}\frac{\alpha_e h_D}{\hat{C}_p T_e}\frac{\tilde{\Gamma}_c}{1+\tilde{\Gamma}_c}\right)_{i,j} \quad (12)$$

Equation 12 accounts for finite surface catalysis through the Dahmkohler number $\tilde{\Gamma}_{c,i,j} \equiv \Gamma_{c,i,j}/(0.47 Sc^{1/3})$ but does not include effects of reactions across the boundary layer.

The bridging function $Z(\Gamma^*)$ in Eq. 9 varies from 0 (equilibrium limit with three body recombination rates much faster than local flow rates) to 1 (frozen limit with three body recombination rates much slower than local flow rates). It is derived from a fundamentally based analysis of the atomic species conservation equations and is given by

$$Z(\Gamma^*) \approx \frac{3\sqrt{1 + 16\Gamma^*_{i,j}/9} - 1}{2 + 4\Gamma^*_{i,j}} \quad (13)$$

where $\Gamma^*_{i,j}$ is a composite Dahmkohler number defined at each surface mesh point by

$$\Gamma^*_{i,j} = \alpha_{e,i,j}\left[\frac{I_1 + 2\tilde{\Gamma}_c I_2 + \tilde{\Gamma}_c^2 I_3}{(1+\tilde{\Gamma}_c)^2}\right]_{i,j} \Gamma_{G,i,j} \quad (14)$$

The integrals I_1, I_2, and I_3 account for integrated effects of reactions across the boundary layer on heating rates. They are tabulated[3] and curve fits are provided.

$$\begin{aligned} I_1 &\approx 4.80(0.50/Sc_w)^{0.45}\theta_w^{0.80(1-\omega)-1.84} \\ I_2 &\approx 1.80(0.50/Sc_w)^{0.12}\theta_w^{0.63(1-\omega)-1.15} \\ I_3 &\approx 0.93(0.50/Sc_w)^{-0.22}\theta_w^{0.41(1-\omega)-0.65} \end{aligned} \quad (15)$$

These integral approximations are valid over a parameter range $0.04 \le \theta_w \le 0.50$ and $-2 \le \omega \le 0$.

In the test problems considered here the bridging function for oxygen recombination Z_O is based on a recombination rate $k_{r,O} = 7.8510^{13} T^{\omega}$ with $\omega = -1.5$. This rate constant was used in earlier work.[3] Other numerical experiments[5] using a recombination rate extracted from Park's kinetic model yielded equivalent results for Z_O. Recombination rates for atomic nitrogen are approximately 1 to 100 times faster than for atomic oxygen, the factor depending on collision partner and temperature. These rates yield values for Z_N of approximately 1 in the test problems, indicating frozen flow. However, inspection of the near wall atom profiles from the CFD baseline solutions show nitrogen recombination far in excess of that predicted by frozen flow. The approximations in the integral boundary-layer theory do not account for two body, exothermic reactions that deplete atomic nitrogen through collisions with molecular oxygen to form NO and O and through collisions with nitric oxide to form N_2 and O. Consequently, the bridging function for nitrogen recombination Z_N was based on an effective rate coefficient $k_{r,N} = 2000 k_{r,O}$ which approximately calibrates the depletion of atomic nitrogen appoaching the wall in a manner consistent with CFD results. The calibration has not been tested outside the test matrix discussed in a later section.

Additional approximations have been employed in Method 1G to simplify extraction of CFD derived quantities. In extracting CFD baseline quantities, the boundary-layer edge is defined as the point where total enthalpy equals 0.995 of total freestream enthalpy. Velocity at the boundary layer edge is taken as the component that is parallel to the surface. Because energy is used as a primary variable and temperature is a derived quantity in the CFD analysis $h - \alpha h_D$ is substituted for $C_p T$ where $\alpha h_D = \sum_s \alpha_s h_{D,s}$ and $(h - \alpha h_D)/(h - \alpha h_D)_e$ is substituted for θ in the above equations. In order to model the catalytic effect of the surface on homogeneous recombination of both nitrogen and oxygen atoms Eq. 9 is modified as follows.

$$\begin{aligned} Q_{w,i,j} = Q_{w,EQ,i,j} + 0.47 Pr_{w,i,j}^{1/3} \Big(& \\ + Z_O \frac{\alpha_{O,e} h_{D,O}}{\hat{C}_p T_e}\left(Le_w^{0.67}\frac{\tilde{\Gamma}_{c,O}}{1+\tilde{\Gamma}_{c,O}} - Le_w^{0.52}\right) & \\ + Z_N \frac{\alpha_{N,e} h_{D,N}}{\hat{C}_p T_e}\left(Le_w^{0.67}\frac{\tilde{\Gamma}_{c,N}}{1+\tilde{\Gamma}_{c,N}} - Le_w^{0.52}\right)\Big)_{i,j} & \end{aligned} \quad (16)$$

The Dahmkohler numbers in Eqs. 3-5 and the dimensional heating in Eq. 10 require evaluation of the rate parameter χ. Parameter χ is itself a function of the boundary-layer coordinate ξ (Eq. 7) and a local flow dimensionality parameter r (Eq. 8). Analytic approximations to these parameters are available in special regions[2] (e.g. stagnation point, windside centerline, swept wing leading edge). However, direct evaluation of the boundary-layer coordinate ξ through Eq. 7 is

a tedious process on a realistic configuration, requiring streamline tracing back to the original attachment point(s). A simpler approach is to solve for the value of χ which yields q_w using boundary-layer edge and wall properties from the baseline CFD solution. The CFD values of q_w implicitly contain the streamline history and local flow dimensionality effects. A Newton iteration works quite efficiently to handle the nonlinear functionality of q_w on χ. This same value of χ is then used in the integral boundary-layer formulation for the new values of catalysis (and wall temperature, if required) to compute the new heating distribution. The approximation for χ ignores integrated effects of changes in surface temperature and density along the surface streamline, but works well in limited tests performed to date.

The Lewis number may be evaluated in a variety of ways, reflecting the uncertainty of modeling multicomponent diffusion with a single parameter in the integral boundary-layer theory. It has been calculated based on the diffusivity of atomic oxygen diffusing in molecular nitrogen and on a number density weighted average of the diffusion coefficients for each species as computed in the CFD algorithm. The weighted averages can be defined to reflect new (predicted) mass fractions at the surface. There is no single formulation which has been found to be consistently better than any other in the matrix of test problems considered here. Consequently, the simplest approach which is to extract the Lewis number directly from the CFD solution has been employed in the results which follow.

In the most general case with high Mach numbers at the boundary-layer edge, viscous dissipation of kinetic energy tends to produce a local maximum temperature within the boundary layer. The higher temperature may lead to dissociation dominated chemistry within the boundary layer. Inclusion of this effect leads to the following correction which may be added to Eq. 12 or 16:

$$\Delta Q_{w,F} \;=\; -0.47 Pr_w^{1/3} \Gamma_D I_D \frac{h_D}{\hat{C}_p T_e} \left[1 - \frac{Le_w \tilde{\Gamma}_c}{1+\tilde{\Gamma}_c} \right] \tag{17}$$

where I_D is a reaction integral, discussed and tabulated by Inger.[2]

Discontinuous Change of Catalysis, Method 2G

More complete details of the following analysis may be found in a companion paper.[1] The post-processing algorithm used to correct for changes in surface heating associated with an abrupt, local change of the surface catalysis model over a hypersonic vehicle is denoted Method 2G. It is assumed that a change in TPS material occurs at a juncture (jump) location ξ_J. Initially, it will also be assumed that the boundary-layer gas phase can be treated as frozen. Upstream and downstream of ξ_J, both α_e and Γ_c are assumed to vary rather slowly compared with α_w itself in the relaxation zone, and hence are approximated by local constants. This approximation for the variation in α_e is supported by CFD results. The constraint on the variation of Γ_c will be relaxed in the numerical formulation of the solution. The theory predicts a variation in α_w under these constraints as

$$\alpha_w \;=\; C\xi^{-(1+\tilde{\Gamma}_c^+)/2} + \frac{\alpha_e}{1+\tilde{\Gamma}_c^+} \qquad (\xi \geq \xi_J) \tag{18}$$

Even though $\tilde{\Gamma}_c$ is discontinuous across the juncture the variation of α_w across the juncture must be continuous (though its gradient will be discontinuous). Consequently, the constant C is proportional to the jump in $\tilde{\Gamma}_c$ and defined by

$$C \;=\; \alpha_e \left(\frac{1}{1+\tilde{\Gamma}_c^-} - \frac{1}{1+\tilde{\Gamma}_c^+} \right) \xi_J^{(1+\tilde{\Gamma}_c^+)/2} \tag{19}$$

Examination of Eqs. 18 and 19 reveals two features of the relaxation process. First, the further downstream the jump is, the longer it takes to adjust to the new catalytic condition. Second, the more catalytic the surface, the shorter the relaxation distance for any imposed $\Delta\Gamma_c$.

The actual variation of $\tilde{\Gamma}_c$ is approximated by treating the boundary of each subsequent computational cell downstream of junction J as a new material interface. The effective upstream Dahmkohler number $\tilde{\Gamma}_c^-$ is then reset to $\alpha_e/\alpha_w - 1$. The value of ξ_J used in Eq. 19 is updated according to the location of the latest interface. These redefinitions, using the previously computed value for α_w from Eq. 18, are consistent with an upstream surface with catalytic efficiency that yields the instantaneous value of α_w in frozen flow. The net effect of this numerical treatment in the subsequent test problem is to produce a faster accomodation (60% reduction in relaxation length) to the new surface catalysis values of heating and mass fraction.

The diffusional contribution to the heat transfer function Q_w will jump discontinuously across the juncture because of the discontinuous change in the gradient $d\alpha_w/d\eta \;=\; \Gamma_c \alpha_w$.

$$\begin{aligned} Q_w \;&= 0.47 Pr^{1/3} \left[1 - \theta_w + \frac{\sqrt{Pr} u_e^2}{2\hat{C}_p T_e} \right] \\ &\quad + \frac{0.47 Sc^{1/3} h_D}{\hat{C}_p T_e} \left[Le \tilde{\Gamma}_c \alpha_w \right] \end{aligned} \tag{20}$$

The application of Eq. 20 in Method 2G to correct CFD baseline results obtained without the local change in surface catalysis follows the example set in Method 1G. Note that in Eq. 20 the first term represents the continuous part of the solution across the juncture and the second part represents the jump effect associated with the diffusional term. When the change in Q_w is computed between the baseline case and the case with

a jump in surface catalytic efficiency the contribution from the continuous part exactly cancels.

Though not presented here, the assumption of frozen gas phase in the boundary layer can be eliminated. In this case, a local iteration is required to account for the sudden change in boundary condition on the reaction integral. Inclusion of this effect was not significant in the test cases which follow.

Test Cases

Tests of Method 1G for hypersonic flow over a 0.6 m radius sphere are presented. Surface heating rates are computed for three different wall catalytic boundary conditions at trajectory points defined in Table 1. The wall temperature in each case is defined by a radiative equilibrium wall boundary condition with emissivity $\epsilon = 0.9$. Grid resolution is 30 cells in the streamwise direction and 64 cells across the shock layer. Cell Reynolds number at the wall in all cases is less than 6. These results differ from those presented earlier[5] in that the current methodology is not restricted to the nose region and the CFD results were all run at their respective radiative equilibrium wall temperatures. A secondary iteration was employed in Method 1G to accomodate the implicit, functional dependence of Γ_c and θ_w on the wall temperature.

Table 1 - Trajectory and Heating

Pt	V_∞,	ρ_∞,	T_∞,	q_1,	q_γ,	q_0,
-	m/s	kg/m^3	K	W/cm^2		
1	5493.	2.00 $^{-4}$	238.	52.1	41.4	25.2
2	4440.	3.53 $^{-4}$	250.	34.6	30.4	20.5
3	3551.	6.64 $^{-4}$	264.	21.8	18.6	14.7

In Fig. 1a, the non-catalytic solution is treated as the available CFD baseline solution. This baseline CFD data set has been post-processed using Method 1G to obtain corrected heating levels associated with changes in the surface catalysis model to finite catalytic and to fully catalytic. The actual CFD heating predictions with the new surface catalysis models are compared with the results of Method 1G in Fig. 1a.

Similar comparisons are made in Fig. 1b for point 1 except that the finite-catalytic CFD solution is used as a baseline and post-processed corrections are derived for the fully catalytic and non-catalytic surfaces. The fully catalytic CFD solution is used as a baseline in Fig. 1c. Comparisons of Method 1G with CFD at successive trajectory points are presented in Fig. 2 for point 2 and Fig. 3 for point 3.

Surface catalysis plays a major role in the stagnation region heating rate in all of the test problems. Method 1G predicts that roughly 56% of the total heating at Point 1 is associated with diffusion of atoms that

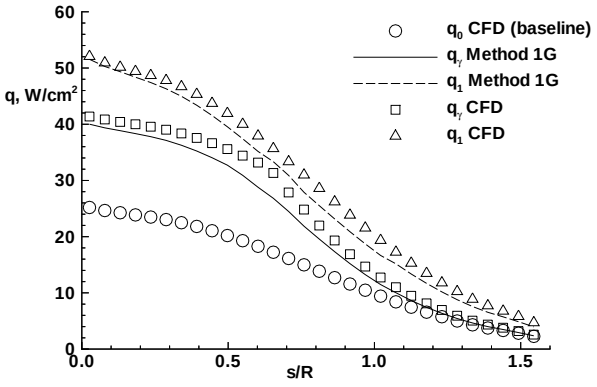

(a) CFD baseline at $\gamma = 0$

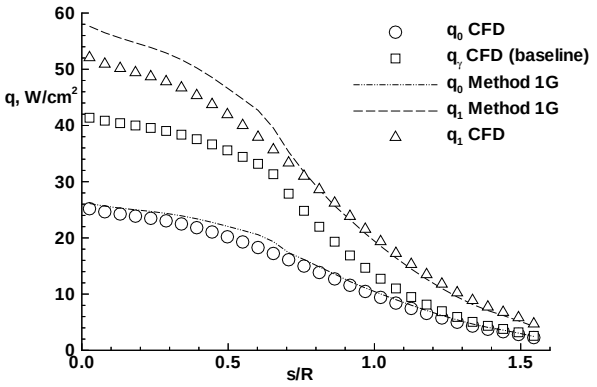

(b) CFD baseline at $\gamma = \gamma(T)$

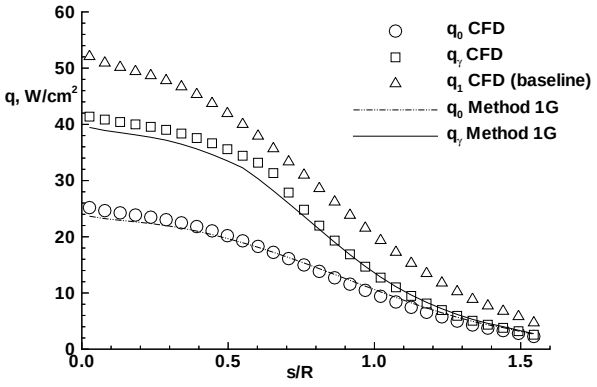

(c) CFD baseline at $\gamma = 1$

Figure 1: Comparison of CFD heating levels (symbols) with Method 1G corrections (lines) derived from CFD baseline for point 1 as function of three surface catalysis models.

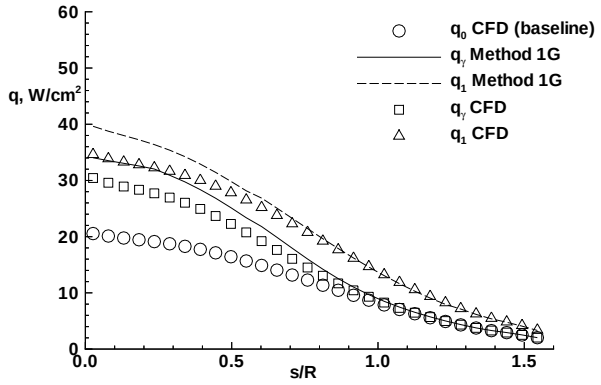

(a) CFD baseline at $\gamma = 0$

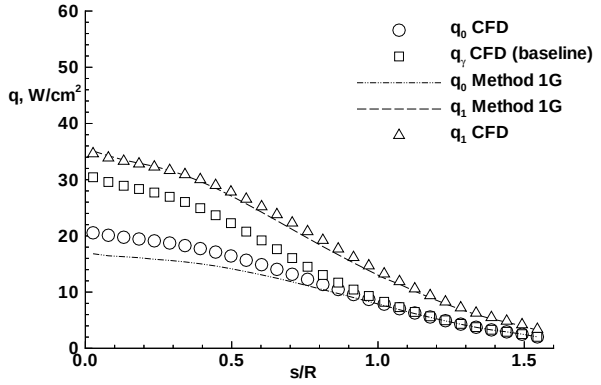

(b) CFD baseline at $\gamma = \gamma(T)$

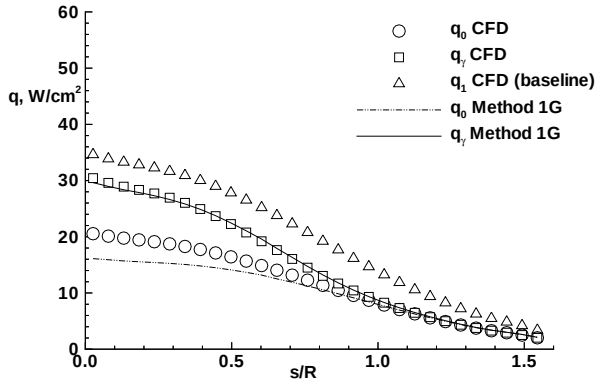

(c) CFD baseline at $\gamma = 1$

Figure 2: Comparison of CFD heating levels (symbols) with Method 1G corrections (lines) derived from CFD baseline for point 2 as function of three surface catalysis models.

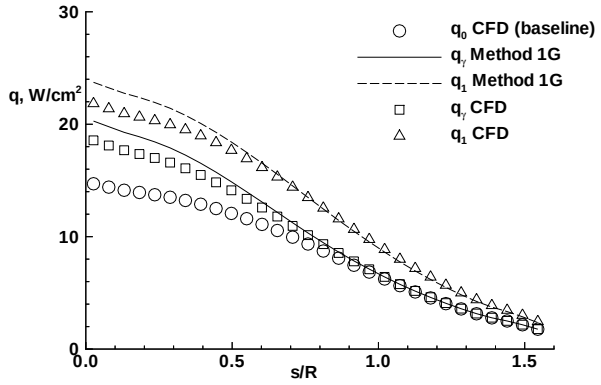

(a) CFD baseline at $\gamma = 0$

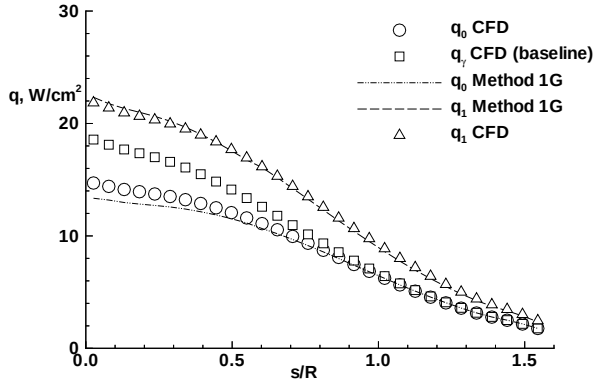

(b) CFD baseline at $\gamma = \gamma(T)$

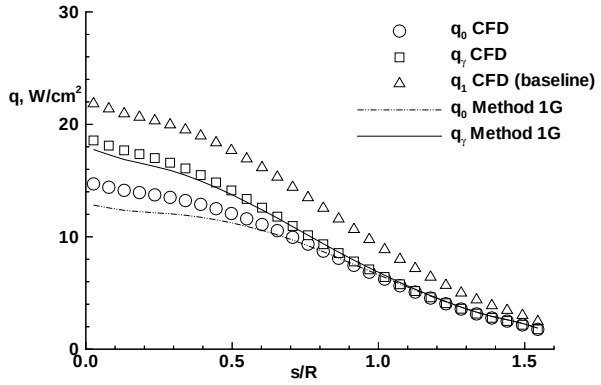

(c) CFD baseline at $\gamma = 1$

Figure 3: Comparison of CFD heating levels (symbols) with Method 1G corrections (lines) derived from CFD baseline for point 3 as function of three surface catalysis models.

recombine at the surface of a fully catalytic wall. In this specific case, approximately 26% of the fully catalytic heating result is associated with diffusion of oxygen atoms to the surface and another 30% with the diffusion of nitrogen atoms to the surface. At Point 2, approximately 40% of the fully catalytic heating result is associated with diffusion of oxygen atoms to the surface and less than 1% with the diffusion of nitrogen atoms to the surface. At Point 3, approximately 33% of the fully catalytic heating result is associated with diffusion of oxygen atoms to the surface and nearly 0% with the diffusion of nitrogen atoms to the surface. The contribution of nitrogen atoms rapidly diminishes as flow expands around the sphere at Point 1 because the mass fraction of atomic nitrogen at the boundary-layer edge goes to zero.

Initial predictions for $\alpha_{N,w}$ at Point 1 using a conventional value for $k_{r,N}$ in Eq. 4 were much larger than CFD results. As noted earlier, the approximations in the integral boundary-layer theory do not account for two body, exothermic reactions that deplete atomic nitrogen through collisions with molecular oxygen to form NO and O and through collisions with nitric oxide to form N_2 and O. These reaction mechanisms also help explain why Method 1G predictions for atomic oxygen near the surface tend to underpredict (5% to 20%) the CFD results when atomic nitrogen exists at the boundary-layer edge. Increasing the value of the effective nitrogen recombination rate coefficient ($k_{r,N} = 2000 k_{r,O}$) approximately models the depletion of atomic nitrogen appoaching the wall in a manner consistent with CFD results.

The large changes in surface heating associated with changes in surface catalysis models are generally well predicted across the test matrix. Nitrogen chemistry plays a major role in the stagnation region at the first trajectory point. Oxygen chemistry is the predominant factor away from the stagnation point and at the stagnation point later in the trajectory. Method 1G predictions are within 7% of CFD results away from the stagnation point ($s/R > 0.8$) in all but one case. The exception, a Point 1 prediction of fully catalytic heating based on a non-catalytic CFD baseline, is within 12% of the CFD result. Stagnation region heating predictions by Method 1G at Point 3, where nitrogen chemistry is not important, are within 10% of CFD results in all but one case. The exception here is for the prediction of non-catalytic heating from a fully catalytic CFD baseline which is within 17% of the CFD result. Stagnation region heating predictions for the first two trajectory points in which nitrogen chemistry begins to play an important role are within 20% of the CFD results.

Application of Method 1G to real design problems are unlikely to involve non-catalytic boundary conditions. Non-catalytic surface specification in the CFD analysis is insufficiently conservative for TPS design purposes, even in cases where low catalytic coatings are used (e.g. shuttle tiles). In cases where nitrogen chemistry plays an active role it is evident in Figs. 1 and 2 that even a little surface catalysis can produce heating levels that are closer to being fully catalytic than non-catalytic. In all cases where Method 1G is used to calculate fully catalytic heating from a finite-catalytic baseline CFD solution, the resultant prediction is within 12% of the CFD result. In all cases where Method 1G is used to calculate finite-catalytic heating from a fully catalytic baseline CFD solution, the resultant prediction is within 5% of the CFD result. Consequently, it is advised that fully catalytic baseline CFD solutions be run early in the design phase of a hypersonic vehicle. This approach yields CFD solutions for laminar, nonequilibrium flows that: (1) are conservative; (2) converge more quickly than with finite- or non-catalytic surface conditions; and (3) provide the best baseline for analytic extrapolation to various TPS design options.

Global Changes to Surface Catalysis - RLV

In this section, application of Method 1G to a relatively complex configuration is tested. The front and mid- sections of a Reusable-Launch-Vehicle (RLV) candidate configuration (Fig. 4) for a flowfield simulation at Mach 25, 45 deg. angle of attack, and 79.6 km altitude is examined. The surface grid representation for the front section is defined with 52 streamise cells and 64 circumferential cells. The surface grid representation for the mid-section is defined with 18 streamwise cells and 77 circumferential cells. The shock layer is resolved with 64 cells. Heating rates for both a fully catalytic wall and a finite-catalytic wall were computed at the respective radiative equilibrium wall temperatures. A secondary iteration was employed in Method 1G to accomodate the implicit, functional dependence of Γ_c

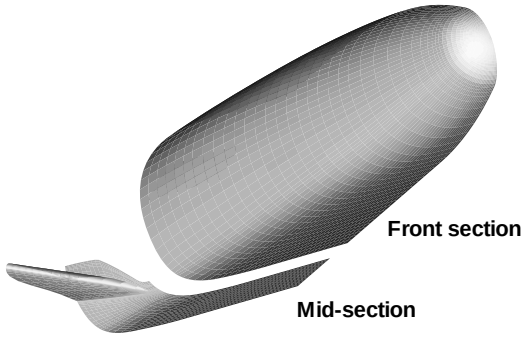

Figure 4: Front and mid-sections of RLV test configuration.

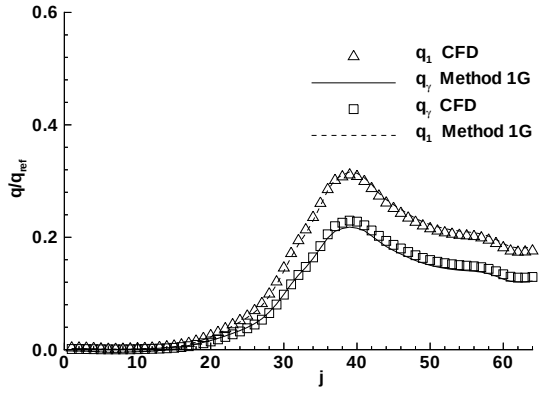

(a) $i = 40$, circumferential distribution

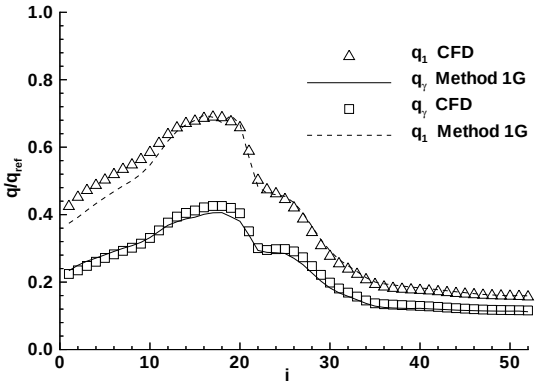

(b) $j = 64$, centerline distribution

Figure 5: Comparison of CFD heating levels obtained on front section of RLV with Method 1G predictions obtained at $\gamma = \gamma(T)$ and $\gamma = 1$ at Mach 25 and 79.6 km.

and θ_w on the wall temperature.

Circumferential heating distributions as a function of computational coordinate j varying from leeside ($j = 1$) to windside ($j = 64$) are presented in Fig. 5a for the front section. The circumferential cut is from the $i = 40$ plane which lies far downstream from the nose and upstream of a wing. The windside centerline heating distribution as a function of computational coordinate i varying from the stagnation point ($i = 16$) to the exit plane of the front section ($i = 52$) is presented in Fig. 5b. Method 1G corrections to CFD baseline heating are generally within 5% of computations. In the earlier version of Method 1G[5] a separate bridging function for nitrogen Z_N was not used and comparisons in the stagnation region were only within 20%.

The mid-section of the RLV (Fig. 4) includes the

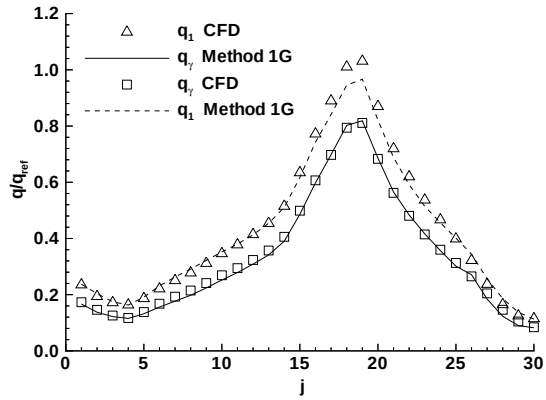

(a) $i = 10$, wing

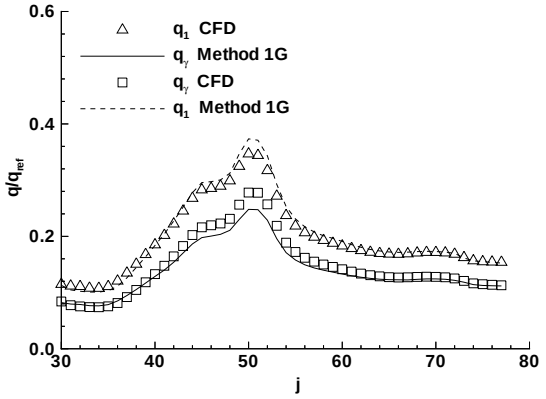

(b) $i = 10$, windside

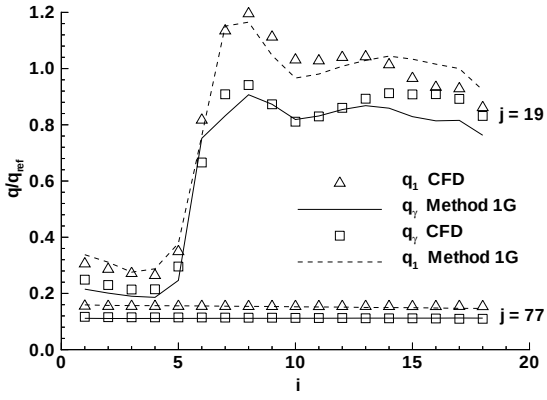

(c) $j = 19, 77$, centerline and wing leading edge

Figure 6: Comparison of CFD heating levels obtained on mid-section of RLV with Method 1G predictions obtained at $\gamma = \gamma(T)$ and $\gamma = 1$ at Mach 25 and 79.6 km.

windside surface, the wing, and a small part of the leeside surface. The CFD and integral-boundary-layer results for heating on this section are compared in Fig. 6. Comparisons are generally within 5% in a circumferential direction around the wing leading edge (Fig. 6a), around the windside surface (Fig. 6b) and in a longitudinal direction along the windside centerline (Fig. 6c). Comparisons along the wing leading edge show differences that are generally less than 10%.

Even in the case where significant turning of streamlines occurs for flow expanding around the side of the vehicle ($32 < j < 48$), in Fig. 5a the integral-boundary-layer extrapolation from the baseline CFD computation is an excellent predictor of the CFD result at the off-baseline catalysis model. Though not shown in the figures, the Method 1G predictions for a non-catalytic surface using either the fully catalytic baseline or the finite-catalytic baseline also agree within a few percent.

The results in Fig. 5 and 6 do not include the correction for dissociation dominated chemistry in the boundary layer as defined in Eq. 17. The correction was evaluated and found to represent less than 1% of the total heating along the windside centerline for this case. The term grew unreasonably large as the leeside was approached. It appears that the curve fits to tabulated data for the reaction integral[2] I_D are used outside their range of validity. It is expected that this term would be of greater significance if the vehicle were at a smaller angle of attack and more dissociation occurred within the boundary layer.

The differences shown for this test case are thought to be small enough to be acceptable for preliminary thermal protection system design purposes. Consistency of these predictions over a broader range of entry conditions and geometric complexity remains to be established before Method 1G (or a related approach) can be used with confidence in a design mode. The calculations presented here using Method 1G offer strong evidence that this design goal is within reach.

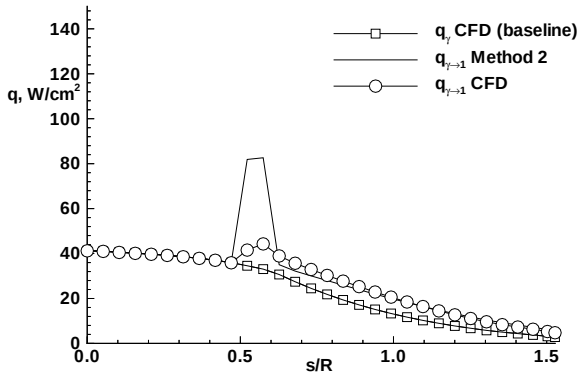

(a) $\Delta s/R = \pi/60$.

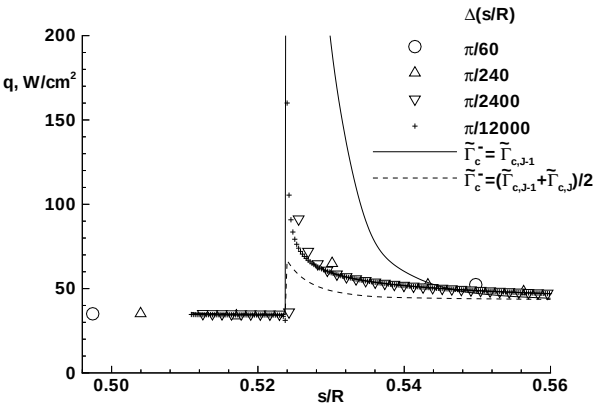

(b) Local grid refinement study

Figure 7: Comparison of CFD heating levels obtained for an abrupt change in surface catalysis from $\gamma = \gamma(T)$ to $\gamma = 1$ with analytic corrections derived from CFD profiles obtained at $\gamma = \gamma(T)$ for point 1.

Discontinuous Changes to Surface Catalysis - Sphere

An abrupt change in surface catalysis (from finite-catalytic to fully catalytic) is introduced on the sphere for trajectory point 1 of Table 1 at $s/R = \pi/6$. Such a change would approximately correspond to use of a glassy coated surface at the stagnation point followed by polished (non-oxidized), metallic surface. The integral boundary-layer methodology is used to predict both the overshoot in heating rate at the juncture and the relaxation distance to the new heating level corresponding to $\gamma = 1$. Wall temperature distributions are held fixed at the radiative equilibrium values corresponding to the finite-catalytic solution. Abrupt changes in surface temperature would introduce additional effects which are not currently modeled in the integral boundary-layer solution.

In Fig. 7, the finite-catalytic solution is treated as the available CFD baseline solution at trajectory point 1. Method 2G is used to post-process the CFD solution to predict the heating levels associated with a local, discontinuous change in surface catalysis to a fully catalytic condition at $s/R = \pi/6$. This result is compared to a corresponding CFD computation with identical wall temperature distribution and grid density. The CFD results in Fig. 7a are computed with 30 cells in 3 degree increments ($\Delta s/R = \pi/60$). This grid density would generally be considered adequate to resolve the flowfield over a hemisphere in the streamwise direction. The integral boundary-layer theory (Method 2)[5] shows a spike in predicted heating level of thickness

equal to one cell and magnitude more than double the upstream location. (The spike is somewhat rounded in Fig. 7a because the plotting routine averages cell centered quantities in order to plot at cell corners. This deficiency is corrected in more recent work presented in Fig. 7b.) The CFD solution shows only a mild overshoot in heating on this grid. While a discontinuous rise in heating is expected across the interface, the relaxation process back down to the fully catalytic level is not properly resolved. The lack of resolution is not a limitation of the theory; rather, the theory is only applied at CFD grid points in the present algorithm.

The CFD solutions are compared on an expanded scale using successively finer grids in Fig. 7b. The finest grid resolves to 0.1571 mm in the streamwise direction. A relaxation process is evident on this scale. The CFD heating overshoot increases by more than a factor of three from the coarsest to finest grid solution. Tests which compared CFD solutions with and without physical diffusion in the streamwise direction show only small perturbations in the solution near the discontinuity on the finest grid. Streamwise grid resolution on the finest grid is on the order of tens of mean free paths at the surface. Cell aspect ratio next to the surface is 18. The Method 2G jump is still approximately a factor of 5 greater than the CFD jump on the finest grid. Further refinement would appear to bring the jump predictions in better agreement; however, physical relevancy of such a simulation is questionable.

The predicted overshoot from Method 2G is extremely sensitive to the ratio of Dahmkohler numbers $\tilde{\Gamma}_c^+/\tilde{\Gamma}_c^-$ across the interface. Unmodified application of Method 2G bounds the CFD result from above. If the effective Dahmkohler number at the upstream side of the juncture is modeled as an average of cell center values on either side of the juncture ($\tilde{\Gamma}_c^- = (\tilde{\Gamma}_{c,J-1} + \tilde{\Gamma}_{c,J})/2$) then the theory bounds the CFD result from below (Fig. 7b dashed line). The impact of uncertainties discussed earlier regarding proper modeling of nitrogen chemistry near the wall has not been investigated. It is suspected to be large because of the demonstrated sensitivity to $\tilde{\Gamma}_c^-$. Review of flight data[19] and additional test cases in which nitrogen recombination is not an additional complicating factor need to be implemented.

The present test case provides an extreme example of the overshoot that can be obtained with abrupt changes in surface catalysis. Usually, the juncture would be placed much further from the stagnation point. Theory shows that the relaxation distance increases with running length from the stagnation point, easing somewhat the necessity for local grid refinement. Nevertheless, the integral-boundary-layer analysis provides a-priori guidance as to the spacial resolution required to computationally address these issues.

Concluding Remarks

A new approach for combining the insight afforded by integral boundary-layer analysis with comprehensive (but time intensive) computational fluid dynamic (CFD) flowfield solutions of the thin-layer Navier-Stokes equations is presented. The approach extracts CFD derived quantities at the wall and at the boundary layer edge for inclusion in a post-processing boundary-layer analysis, valid for most of the acreage on a realistic hypersonic vehicle. It allows a designer at a workstation to address two questions, given a *single*, baseline CFD solution: (1) How much does the heating change for a thermal protection system with different catalytic properties than was used in the baseline CFD solution? (2) How does the heating change at the interface of two different TPS materials with an abrupt change in catalytic efficiency?

Global changes in surface catalysis lead to global changes in heating rates. Method 1G is a straightforward extension of Method 1 which is applicable to the entire vehicle. Rather than employing limiting forms of the boundary-layer equations or integrating along streamlines, it solves for an integral-boundary-layer streamline parameter to match the local CFD baseline heating rate. This parameter is then used to predict heating rates at off-baseline values of surface catalysis. Off-baseline predictions of heating rates by Method 1G were generally in very good agreement with CFD solutions.

Some additional tuning of the method may still be required as the role of nitrogen atoms predominates the role of oxygen atoms in the diffusional component of catalytic heating. Also, the consistency of these predictions over a broader range of entry conditions and geometric complexity remains to be established before Method 1G (or a related approach) can be used with confidence in a design mode. The calculations presented here using Method 1G offer strong evidence that this design goal is within reach.

It is advised that fully catalytic baseline CFD solutions be run early in the design phase of a hypersonic vehicle. This approach yields CFD solutions for laminar, nonequilibrium flows that: (1) are conservative; (2) converge more quickly than with finite- or non-catalytic surface conditions; and (3) provide the best baseline for analytic extrapolation to various TPS design options.

Abrupt, discontinuous changes in surface catalysis lead to large, local changes in heating rates that must relax to the new level dictated by the catalytic efficiency of the new surface. Method 2G predicted large heating spikes associated with an abrupt change in surface catalysis. The spikes were much larger than initially predicted by CFD. However, the relaxation zone,

as defined by the integral-boundary-layer method, was not adequately resolved, and grid refinement ultimately increased the CFD heating spike by a factor of three. Still, theoretical results are extremely sensitive to the ratio of catalytic Dahmkohler numbers across the discontinuity. CFD results are extremely sensitive to the streamwise grid resolution. The theory gives good a-priori guidance on the extent of the relaxation downstream of the singularity, but additional research is required to resolve differences in predicted magnitudes in the heating jump.

References

[1]Inger, G. R., and Gnoffo, P. A., "Hypersonic Entry Heating with Discontinuous Surface Catalycity: A Combined Analytic/CFD Approach," AIAA Paper 96-2150, June 1996.

[2]Inger, G. R., "Nonequilibrium Boundary Layer Effects on the Aerodynamic Heating of Hypersonic Waverider Vehicles," *Journal of Thermophysics and Heat Transfer*, Vol. 9, No. 4, October-December 1995, pp. 595–604.

[3]Inger, G. R., "Nonequilibrium Stagnation Point Boundary Layers with Arbitrary Surface Catalycity," *AIAA Journal*, Vol. 1, No. 8, August 1963, pp. 1776–1784.

[4]Inger, G. R., and Elder, J., "Recombination Dominated Nonequilibrium Heat Transfer to Arbitrarily Catalytic Hypersonic Vehicles," *Journal of Thermophysics and Heat Transfer*, Vol. 5, No. 4, 1992, pp. 449–455.

[5]Gnoffo, P. A., "Analytic Corrections to CFD Heating Predictions Accounting for Changes in Surface Catalysis," AIAA Paper 96-1800, June 1996.

[6]Gnoffo, P. A., "Point-Implicit Relaxation Strategies for Viscous, Hypersonic Flows," in *Computational Methods in Hypersonic Aerodynamics* (Murthy, T. K. S., ed.), Computational Mechanics Publications, pp. 115–151, Kluwer Academic Publishers, 1991.

[7]Gnoffo, P. A., "Upwind-Biased, Point-Implicit Relaxation Strategies for Viscous, Hypersonic Flows," AIAA Paper 89–1972, 1989.

[8]Gnoffo, P. A., "An Upwind-Biased, Point-Implicit Relaxation Algorithm for Viscous, Compressible Perfect-Gas Flows," NASA TP 2953, February 1990.

[9]Gnoffo, P. A., "Code Calibration Program in Support of the Aeroassist Flight Experiment," *Journal of Spacecraft and Rockets*, Vol. 27, No. 2, March-April 1990, pp. 131–142.

[10]Weilmuenster, K. J., and Gnoffo, P. A., "Aeroassisted Flight Experiment Aerodynamic Characteristics at Flight Conditions," *Journal of Spacecraft and Rockets*, Vol. 27, No. 6, November-December 1990, pp. 684–686.

[11]Thompson, R. A., and Gnoffo, P. A., "Application of the LAURA Code for Slender Vehicle Aerothermodynamics," *Journal of Spacecraft and Rockets*, Vol. 29, No. 1, January-February 1992, pp. 16–23.

[12]Weilmuenster, K. J., Gnoffo, P. A., and Greene, F. A., "Navier-Stokes Simulations of Orbiter Aerodynamic Characteristics Including Pitch Trim and Bodyflap," *Journal of Spacecraft and Rockets*, Vol. 31, No. 3, May-June 1994, pp. 355–366.

[13]Gnoffo, P. A., Weilmuenster, K. J., and Alter, S. J., "Multiblock Analysis for Shuttle Orbiter Reentry Heating from Mach 24 to Mach 12," *Journal of Spacecraft and Rockets*, Vol. 31, No. 3, May-June 1994, pp. 367–377.

[14]Roe, P. L., "Approximate Riemann Solvers, Parameter Vectors, and Difference Schemes," *Journal of Computational Physics*, Vol. 43, October 1981, pp. 357–372.

[15]Harten, A., "High Resolution Schemes for Hyperbolic Conservation Laws," *Journal of Computational Physics*, Vol. 49, No. 2, February 1983, pp. 357–393.

[16]Yee, H. C., "On Symmetric and Upwind TVD Schemes," NASA TM 88325, 1986.

[17]Stewart, D. A., Leiser, D. B., Kolodziej, P., and Smith, M., "Thermal Response of Integral Multicomponent Composite Thermal Protection Systems," AIAA Paper 85–1056, June 1985.

[18]Goulard, R. J., "On Catalytic Recombination Rates in Hypersonic Stagnation Heat Transfer," *Jet Propulsion*, Vol. 28, No. 11, 1958, pp. 737–745.

[19]Rakich, J. V., Stewart, D. A., and Lanfranco, M. J., "Results of a Flight Experiment on the Catalytic Efficiency of the Space Shuttle Heat Shield," AIAA Paper 82–0944, June 1982.